Article:
Marin-Beloqui, J.M., Toolan, D.T.W., Panjwani, N.A. et al. (2021) Triplet-charge annihilation in a small molecule donor: acceptor blend as a major loss mechanism in organic photovoltaics. Advanced Energy Materials, 11 (24). 2100539. ISSN: 1614-6832

https://doi.org/10.1002/aenm.202100539

ADVANCED ENERGY MATERIALS
www.advenergymat.de

Triplet-Charge Annihilation in a Small Molecule Donor: Acceptor Blend as a Major Loss Mechanism in Organic Photovoltaics

Jose M. Marin-Beloqui, Daniel T. W. Toolan, Naitik A. Panjwani, Saurav Limbu, Ji-Seon Kim, and Tracey M. Clarke**

Organic photovoltaics (OPV) are close to reaching a landmark 20% device efficiency. One of the proposed reasons that OPVs have yet to attain this milestone is their propensity toward triplet formation. Herein, a small molecule donor, DRCN5T, is studied using a variety of morphology and spectroscopy techniques, and blended with both fullerene and non-fullerene acceptors. Specifically, grazing incidence wide-angle X-ray scattering and transient absorption, Raman, and electron paramagnetic resonance spectroscopies are focused on. It is shown that despite DRCN5T's ability to achieve OPV efficiencies of over 10%, it generates an unusually high population of triplets. These triplets are primarily formed in amorphous regions via back recombination from a charge transfer state, and also undergo triplet-charge annihilation. As such, triplets have a dual role in DRCN5T device efficiency suppression: they both hinder free charge carrier formation and annihilate those free charges that do form. Using microsecond transient absorption spectroscopy under oxygen conditions, this triplet-charge annihilation (TCA) is directly observed as a general phenomenon in a variety of DRCN5T: fullerene and non-fullerene blends. Since TCA is usually inferred rather than directly observed, it is demonstrated that this technique is a reliable method to establish the presence of TCA.

1. Introduction

Organic photovoltaics (OPV) have improved notably in efficiency in the last few years, reaching over 18% in single junction devices.[1,2] Despite this rapid enhancement, there are still several aspects in these devices' functions that are not completely understood. Triplet behavior in organic solar cells is one of the most understudied aspects. The reason of the relatively low number of studies is that triplet formation is typically considered a loss pathway, and thus associated with systems with low device efficiencies. Indeed, many previous studies indicated that triplets were formed only when charge separation did not occur or was very inefficient.[3–6] As such, triplets were considered irrelevant for the highest efficiency OPV devices. However, it has recently been demonstrated that OPV blends with non-fullerene acceptors (NFAs), the main driver of the current record OPV efficiencies, can show pronounced triplet formation and yet still provide high efficiencies.[7] In the benchmark PM6:Y6 blend, for example, NFA triplet exciton formation accounts for 90% of charge recombination at open circuit, leading to a 60 mV reduction of the open circuit voltage. As such, it is important to elucidate triplet pathways in organic solar cells, in particular how they affect charge photogeneration and recombination.

Triplets can be generated via several different pathways in organic solar cells.[8,9] First, the photogenerated singlet exciton can undergo intersystem crossing (ISC). Second, triplets can form via charge transfer (CT) states at the donor/acceptor interface. These CT states can undergo rapid spin-mixing due to the low exchange energy between ^{3}CT and ^{1}CT states, often

Dr. J. M. Marin-Beloqui, Dr. T. M. Clarke
Department of Chemistry
University College London
Christopher Ingold Building, London WC1H 0AJ, UK
E-mail: j.beloqui@ucl.ac.uk; tracey.clarke@ucl.ac.uk

The ORCID identification number(s) for the author(s) of this article can be found under https://doi.org/10.1002/aenm.202100539.

DOI: 10.1002/aenm.202100539

Dr. D. T. W. Toolan
Department of Chemistry
The University of Sheffield
Sheffield S3 7HF, UK

Dr. N. A. Panjwani
Berlin Joint EPR Lab
Fachbereich Physik
Freie Universität Berlin
D-14195, Berlin, Germany

S. Limbu, Prof. J.-S. Kim
Department of Physics and Centre for Processable Electronics
Imperial College London
London SW7 2AZ, UK

leading to an equilibrium between these two states.[10–12] The ^{3}CT states can undergo back recombination, leading to the formation of a triplet localized on either donor or acceptor.[13–16] Importantly, this process can happen during the initial charge photogeneration process (geminate triplet formation) or during the bimolecular recombination of separated polarons, which can also occur via a CT state (non-geminate triplet formation).[12,17,18] However, when triplet formation originates from non-geminate polaron recombination, triplet formation may not affect the device short-circuit current,[19] particularly in cases with high charge carrier mobilities. Charges can then be extracted prior to recombination and, hence, triplet formation.

Indeed, despite triplets usually being categorized as a loss pathway in solar cells, several reports have noted an enhancement in efficiency with a higher population of triplet species.[20–22] Remarkably, there are some solar cells that operate by harvesting triplet excitons rather than singlets.[23–27] Such devices, typically relying on heavy transition metals, exploit the longer diffusion length and lifetimes of triplets (compared to singlets) to enhance the photocurrent. Despite the efficiency of these triplet solar cells being relatively low, these reports make an important point: it is possible to extract actual energy from triplet species. Furthermore, Laquai et al. showed that triplets could create polarons through triplet-triplet annihilation (TTA), enhancing the maximum theoretical efficiency.[28] As result of the TTA process, new high energy singlets were created. These singlet excitons had enough energy to undergo delayed charge separation on the nanosecond timescale. In addition, it was found these charges had longer lifetimes as they were not immediately lost to nongeminate recombination (due to the smaller charge population present at longer times).

The lack of full understanding of triplet formation and behavior, as well as their potential in enhancing OPV device efficiency, necessitates more fundamental studies. Herein, we provide an in-depth spectroscopy study of triplets focusing on transient absorption spectroscopy (TAS), both in the picosecond and microsecond regimes. TAS is a pump-probe technique that allows transient species such as singlets, polarons, and triplets to be probed directly. A main advantage of TAS is that the TA amplitude signal is directly proportional to the population of the photogenerated species. The amplitude of the polaron TA signal at 1 µs is proportional to both the short circuit current[29] and external quantum efficiency of a photovoltaic device.[30]

In this work, we have used a variety of spectroscopy and morphology techniques to study donor/acceptor blends with DRCN5T, (2, 2′-((5Z, 5′Z)–5, 5′–((3, 3‴, 3‴′, 4′–tetraoctyl–[2, 2′:5′, 2″:5″, 2‴:5‴, 2‴′–quinquethiophene]–5, 5‴′diyl) bis (methanylylidene)) bis (3-ethyl-4-oxothiazolidine-5, 2-diylidene)) dimalononitrile), a donor small molecule that produces a large change in solar cell efficiency upon thermal annealing: from 3% to over 8% PCE.[31–33] Noticeably, DRCN5T:PC70BM blends show over 10% efficiencies,[32] close to the 11% record for PC70BM single-junction solar cells.[34,35] Also, DRCN5T has shown efficiencies close to 11% when blended with NFAs[36] and is widely used as a material in ternary blends given its near infrared absorption, recently obtaining almost 17% solar cell efficiency.[31,37–40] In addition, DRCN5T has attracted special attention given its stability versus oxygen, especially after thermal annealing.[41,42] It is also able to increase PC70BM air and light stability, showing negligible short-circuit current loss.[43] Of particular interest for us is the large morphological changes that are induced upon thermal annealing of DRCN5T,[32,42,44] and the motivation for this work is to investigate how such drastic changes influence the interplay between charge carriers and triplets.

Intriguingly, TAS results show that thermal annealing of DRCN5T:PC70BM blends suppress charge carrier formation, despite the known ability of annealing to enhance device efficiencies in this material. The larger, more crystalline DRCN5T domains that form upon annealing are not active in charge photogeneration. However, an enhancement in photoluminescence (PL) upon annealing may enable photon recycling under device conditions, and this could be a significant factor regarding the enhanced device efficiencies.

We also show that DRCN5T blends produce a large triplet population due to back recombination from CT states in amorphous regions, despite the high reported solar cell efficiencies. Moreover, we demonstrate the existence of an additional loss pathway associated with the existence of triplets: triplet-charge annihilation (TCA). Triplet formation is thus detrimental for DRCN5T solar cell efficiency for two reasons: it hinders polaron formation and annihilates the already formed polarons. We demonstrate the generality of this TCA by blending DRCN5T with a variety of fullerene and NFAs. Our direct observation of TCA using µs-TAS under oxygen conditions thus establishes a reliable method to check for the existence of TCA: a loss mechanism rarely considered by the OPV community. Our observations of pronounced triplet formation and triplet-related loss mechanisms in such a high-efficiency blend have profound implications for further enhancements in OPV device performance. A greater, quantitative, consideration of the impact of triplets on device efficiency is needed, in addition to new strategies to alleviate TCA.

2. Results and Discussion

2.1. Steady State Absorbance and PL

Figure 1 shows the ground absorbance spectrum of the DRCN5T films fabricated for the study. The pristine as-spun (unannealed) DRCN5T film shows a broad unresolved absorbance at 600 nm. The blend of DRCN5T with PC70BM causes a 0.14 eV blue shift of the absorbance maximum to 550 nm. This blue-shift may indicate that the introduction of the fullerene causes a distortion in the crystal lattice of the DRCN5T domains, similar to that reported in other materials.[45–47] To restore the crystallinity of the blend film, thermal annealing was performed for 20 min at 120 °C: these conditions are known to enhance OPV efficiency in DRCN5T:PC70BM blends.[31,32] This resulted in pronounced changes to the absorption spectrum, with the appearance of a significantly red-shifted absorption peak at 700 nm. The intensity enhancement of this 0-0 vibronic peak intensity typically indicates an improved crystallinity: the more rigid morphology inhibits structural change during electronic excitation.

Curiously, the annealed DRCN5T:PC70BM absorption spectrum indicates a greater crystallinity compared to the pristine DRCN5T film. This implies that DRCN5T films fabricated by spin-coating, even pristine DRCN5T, form amorphous DRCN5T domains. To confirm this, the pristine sample was annealed in

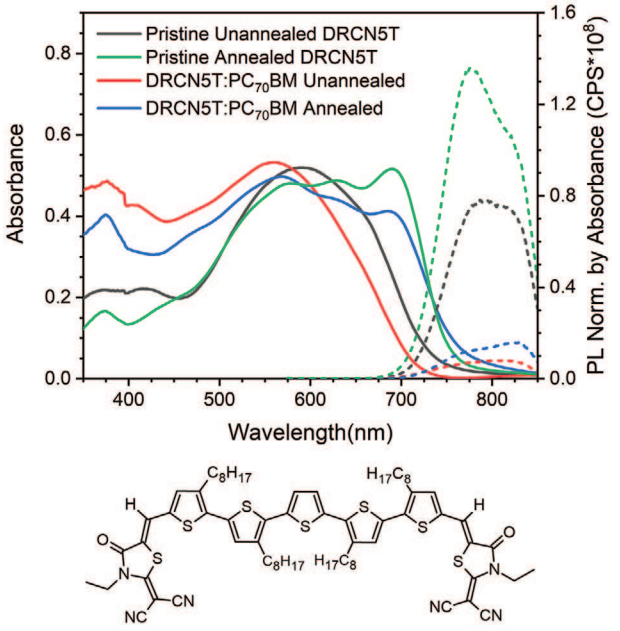

Figure 1. Ground state absorbance (solid lines) and photoluminescence spectra (dotted lines) of unannealed (black) and annealed (green) pristine DRCN5T and unannealed (red) and annealed (blue) DRCN5T:PC70BM 1:0.8 blend films. Photoluminescence was measured via excitation at 550 nm and corrected for absorbance at that wavelength. The structure of DRCN5T is also shown.

similar fashion to the annealed blend, and similar effects on the ground state absorbance were obtained (a large enhancement of the 0-0 vibronic peak at 700 nm). It is noticeable that with the same annealing conditions, the relative intensity of the 700 nm band is higher in the annealed pristine sample than in the annealed blend sample. This indicates a lower crystallinity in the annealed blend sample compared to the annealed pristine, as expected due to the disruption of molecular packing by the PC70BM. Nevertheless, annealing clearly produces large morphological changes upon annealing, for both pristine and blend films.

Figure 1 also shows the PL data of the samples studied. DRCN5T shows a PL band centered at 800 nm, in accordance with previous reports in literature.[42] After annealing, the pristine sample increases in PL intensity by 70%. This pronounced enhancement in the PL intensity can be explained by the large improvement in DRCN5T crystallinity: rigidly planar molecules tend to have greater fluorescence quantum yields due to the deactivation of non-radiative relaxation.

The unannealed and annealed DRCN5T blend samples both show identical relative PL quenching of 89% with the introduction of PC70BM, despite the annealed blend having higher PL than the unannealed one (the quenching of the annealed blend was calculated with the annealed pristine sample as the reference). This decrease in PL signal is associated with exciton quenching in the blend via electron transfer at the donor/acceptor interface. Annealing is usually associated with an increase of domain size and crystallinity. The lack of change in PL quenching with annealing therefore indicates that, despite larger and more crystalline DRCN5T domains (as also suggested by absorbance experiments), the accumulative quenching of the DRCN5T excitons is still quite efficient.

2.2. Grazing Incidence Wide-Angle X-Ray Scattering

Grazing incidence wide-angle X-ray scattering (GIWAXS) was performed to confirm the steady state spectroscopy results and provide greater detail on the morphology of the DRCN5T and DRCN5T:PC70BM blends, with data shown in **Figure 2**. For the as-cast DRCN5T film, the 100 Debye–Sherrer-ring is observed at 0.35 $Å^{-1}$ with higher order reflections (200 and 300) just about visible in the 2D scattering patterns and the radially integrated data. Such scattering features correspond to lamellar stacking of the thiophene backbones, with an interchain spacing of ≈18 Å. An azimuthal integration (Figure S1, Supporting Information) of the 100 Debye–Sherrer-ring clearly shows a maximum at 0°, indicating that the DRCN5T backbone predominantly adopts an edge-on configuration. Upon thermal annealing, the intensity of the h00 reflections significantly increases, with some diffraction spots becoming faintly visible; these observations are indicative of the formation of highly crystalline morphologies. For the DRCN5T:PC70BM blends (both as-cast and annealed) the scattering features at 0.35, 0.64, and 0.98 $Å^{-1}$ are weaker than for the pure DRCN5T films, indicating that the addition of PC70BM perturbs the crystallization of DRCN5T. Upon thermal annealing of the DRCN5T:PC70BM blend, the structure evolves to a similar extent as the pristine unannealed DRCN5T film. The scattering data presented here for the pristine DRCN5T and DRCN5T:PC70BM blends are consistent with the recent in-depth morphological investigations and resultant structural model presented by Berlinghof et al.[48] on DRCN5T:PC70BM blend films.

2.3. Raman Spectroscopy

Another methodology to assess the large morphological changes observed upon annealing for DRCN5T is Raman spectroscopy. Raman spectroscopy is extremely sensitive to small structural and conformational changes of a molecule, and thus is ideal for this purpose. **Figure 3**a shows the Raman spectra of the studied samples, exciting at 457 nm. In all cases, the spectra were dominated by DRCN5T bands, with the most prominent features in the 1400–1500 cm^{-1} region, and smaller bands at 1540, 1590, and 1720 cm^{-1}. A PC70BM band is present in both blends at 1565 cm^{-1}, marked with an asterisk in Figure 3a.[49] In the unannealed pristine and blend samples, a broad C=C stretching mode at 1435 cm^{-1} dominates the spectrum, the large full width at half maximum (FWHM) consistent with the more amorphous nature of these films. Upon annealing the DRCN5T:PC70BM blend film, this 1435 cm^{-1} feature changes considerably, with a large reduction in relative intensity of the shoulder present at 1460 cm^{-1} and a new, sharper, band present at 1425 cm^{-1}. The same behavior is observed in the annealed pristine sample.

DFT calculations (B3LYP/631G(d)) were performed to assign the Raman spectrum vibrational modes and assist with data analysis. The DRCN5T Raman spectra of two different conformations, a fully planar and a more distorted conformation, were calculated (Figure S2, Supporting Information). The distorted conformer shows a single prominent C=C stretching mode localized on the central thiophene rings at 1410 cm^{-1}. The identical mode is demonstrably downshifted to 1400 cm^{-1}

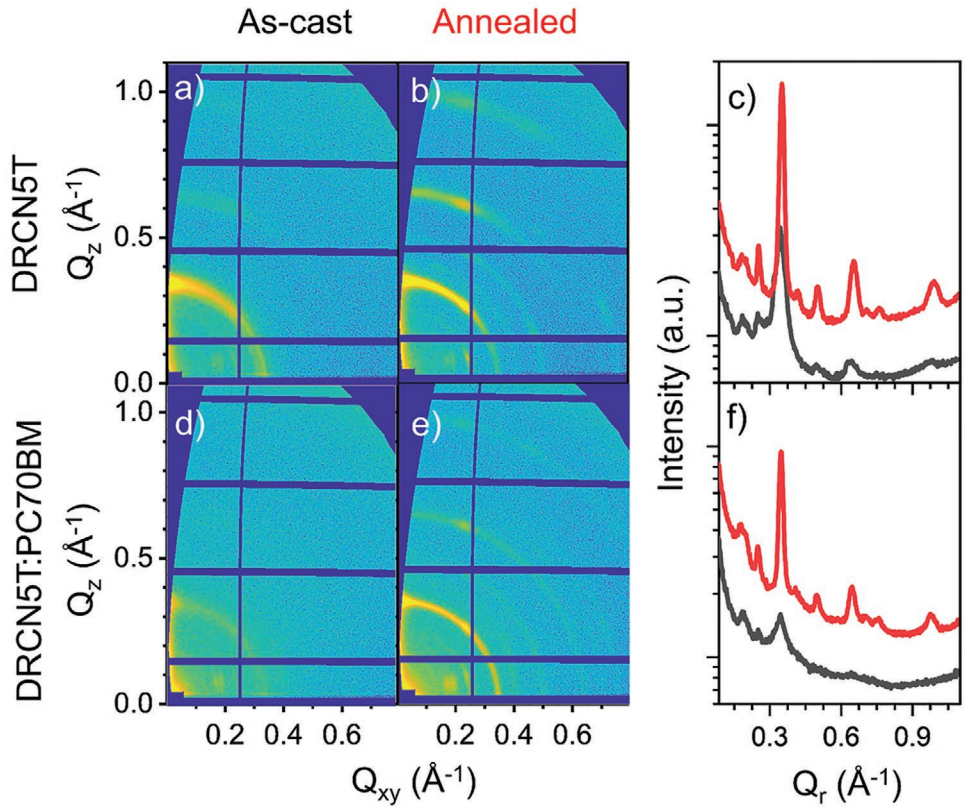

Figure 2. 2D GIWAXS patterns for a,b) pristine DRCN5T and d,e) DRCN5T:PC70BM films, a,d) pre- and b,e) post-annealing. Corresponding radial integrated scattering data is shown for c) pristine DRCN5T and f) DRCN5T:PC70BM, as-cast (black line) and annealed (red line).

in the planar conformer, due to a greater delocalization of the π-electron density along the DRCN5T conjugated backbone, lowering the effective force constant of this vibration.[50–53] We can therefore assign the appearance of the intense, sharp 1425 cm^{-1} peak after annealing to a conformational change of a high percentage of DRCN5T molecules toward a more planar structure. This data indicates a considerable increase in crystallinity upon annealing (as suggested by the steady state absorption spectra and GIWAXS data), but the remaining 1435 cm^{-1} band indicates that some twisted DRCN5T conformers (amorphous regions) still exist after annealing.

Indeed, it is likely that a range of different twisted conformations can exist in the as-spun films, introducing more amorphous nature. The most pronounced amorphous nature is found in the unannealed blend film: it has the largest FWHM of the 1435 cm^{-1} band (38 cm^{-1} compared to 34 cm^{-1} in the unannealed pristine film), caused by greater Raman intensity in its higher energy shoulder (≈1460 cm^{-1}). This high energy shoulder could therefore possess vibrational modes belonging to much more twisted conformers, due to the additional crystallinity disruption caused by the PC70BM. Notably, this high energy region loses almost all of its intensity upon annealing the blend, which is consistent with the higher degree of planarity observed. The rest of the bands are discussed in Figure S3, Supporting Information.

Figure 3b shows the annealed DRCN5T:PC70BM blend Raman spectra as a function of the excitation wavelength (the rest of the studied samples are depicted in Figure S4, Supporting Information). The purpose of this was to use the resonance Raman effect to investigate the observed structural changes in more detail. The resonance Raman effect occurs when the Raman excitation wavelength matches with a particular electronic transition. This enhances the intensity of those vibrational modes that mimic the structural changes associated with the resonant electronic transition.[54–56] In the case of DRCN5T, absorbance at longer wavelengths up to the absorption edge is related to more crystalline DRCN5T domains, and, hence, the vibrational modes associated to these more crystalline domains will be enhanced compared with more amorphous ones.[57] The FT-Raman spectrum measured with 1064 nm excitation corresponds to the non-resonance condition. The DRCN5T C=C stretching modes (centered around 1435, 1545, and 1590 cm^{-1}) progressively downshift 5–10 cm^{-1} with longer excitation wavelengths. This decrease in wavenumber is associated with a decrease in the effective force constant of the double bonds due to a higher delocalization of the π-electron density, and is consistent with the 457 nm excitation data as a function of morphology in Figure 3a.

2.4. Microsecond TAS

Normalized (per photon absorbed) microsecond transient absorption spectra for unannealed and annealed films of pristine DRCN5T and DRCN5T:PC70BM (1:0.8) blend films are shown in **Figure 4**a (full spectra normalized to 1 are shown in Figure S5, Supporting Information). Under inert conditions,

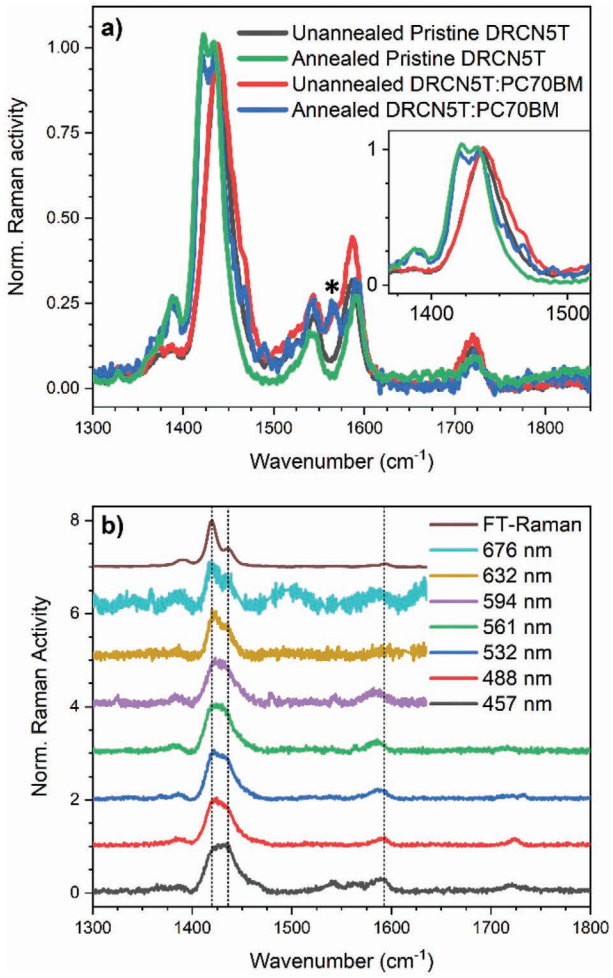

Figure 3. a) Raman spectra of unannealed (black) and annealed (green) pristine DRCN5T, and unannealed (red) and annealed (blue) DRCN5T:PC70BM blend films, excited at 457 nm with a power of 0.1 mW. The asterisk marks the PC70BM Raman band. b) Raman spectra of annealed DRCN5T:PC70BM film recorded with different excitation wavelengths from 457 to 632 nm at 0.1 mW (676 nm spectrum was recorded at 0.2 mW). The FT-Raman spectrum (brown) was added to highlight the resonance Raman effect. Vertical dashed lines were placed to help the eye with the bands of interest.

the unannealed pristine DRCN5T TA spectrum at 1 µs shows a band centered at 1100 nm, which redshifts by 20 nm upon annealing. Both blends also exhibit this peak around 1100 nm, where annealing again causes a small red-shift. This red-shift is likely to be related to the higher crystallinity induced by annealing. For both blend films, the amplitude of the 1100 nm band is higher than in the pristine. Furthermore, the unannealed blend also shows the presence of an additional band at 1600 nm and a more pronounced 950 nm shoulder.

To assign these TA spectral features, the evolution of the spectra over time was assessed. Both pristine films and the annealed blend (Figure S6a,b, Supporting Information, and Figure 4c, respectively) show negligible spectral evolution over time, suggesting that only a single transient species is present. However, this is not the case for the unannealed blend (Figure 4b), for which the 950 nm shoulder and 1600 nm bands decay at the same rate and considerably more slowly compared to the 1100 nm band. This therefore suggests the presence of two species: one which absorbs primarily at 1100 nm, and a second species with a dual absorption at 950 and 1600 nm.

To identify the transient species in each DRCN5T film, oxygen sensitivity experiments were conducted to check for the presence of triplets. In all samples, the presence of oxygen led to a strong and, importantly, a reversible reduction in the amplitude and lifetime of the 1100 nm band, suggesting that this band can be assigned to the triplet state (Figure S7, Supporting Information). The presence of triplets in the film is consistent with TA of the pristine DRCN5T solution (Figure S8, Supporting Information), which shows an oxygen-sensitive band at 950 nm that decays monomolecularly and thus is assigned to triplets. This indicates the suitability of DRCN5T to generate triplets, noting that the shift in triplet absorption (0.18 eV) from solution to condensed phase is commensurate with the shift in ground state absorption (0.25 eV).

The identity of the remaining TA absorption bands at 950 and 1600 nm in unannealed DRCN5T:PC70BM are therefore likely to be related to a charged species. These bands are observed at identical wavelengths when DRCN5T:PC60BM was examined (Figure S9, Supporting Information), and thus can be assigned to DRCN5T positive polarons rather than fullerene features. To support this assignment, TD-DFT calculations (B3LYP/6-31G(d)) of the optical transitions for DRCN5T triplets and polarons were performed. Figures S10 and S11, Supporting Information, show the calculated absorbance spectra and assignments of DRCN5T positive polaron and triplets on a single in vacuo DRCN5T molecule. The triplet absorbance shows a strong band at around 935 nm and a weak band below 600 nm, while the polaron absorbance spectrum shows two strong bands at 800 and 1500 nm, and a weak band at 650 nm. Despite the actual wavelength values obtained through this method not being completely accurate, the relative band positions have been demonstrated to be useful in literature.[58–62] The TD-DFT results presented here support the spectral assignment for DRCN5T, where the single measured absorption band at 1100 nm can be assigned to the triplet (calculated position 935 nm) while the dual bands measured at 950 and 1600 nm can be attributed to the DRCN5T positive polaron (calculated positions 800 and 1500 nm). Note that the third calculated polaron absorption band at 650 nm is apparent in the measured spectrum as another shoulder at 850 nm. The calculated band of the triplet below 600 nm is not visible experimentally as it was obscured by the ground state bleaching. As such, these DFT results support the experimental observation that the TA spectrum obtained in the unannealed blend under inert atmosphere is a combination of both of DRCN5T triplets and polarons, whilst the annealed blend appears to only exhibit triplets.

We thus have three independent experiments demonstrating the presence of triplets in DRCN5T:PC70BM blends: µs-TAS under oxygen, DFT calculations, and EPR (vide infra). However, this pronounced triplet presence in such a high efficiency blend is very unusual, and thus we conduct sensitization experiments to further verify the assignment of the µs-TA 1100 nm band to triplets. The sensitization experiments consist of blending DRCN5T in films with the well-known triplet sensitizer platinum octaethylporphyrin (PtOEP). By photoexciting

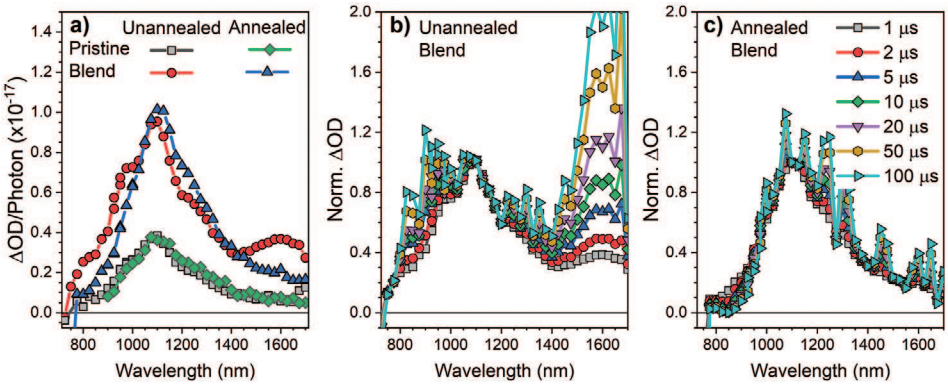

Figure 4. a) Transient absorption spectra at 1 μs normalized per photon absorbed of unannealed (black squares) and annealed (green diamonds) pristine DRCN5T and unannealed (red circles) and annealed (blue triangles) DRCN5T:PC70BM (1:0.8) blend films under nitrogen. Normalized TA spectra recorded over a time range from 1 to 100 μs for b) unannealed and c) annealed blend samples. Spectra were recorded with a pump wavelength of 500 nm, at 10 μJ cm^{-2} excitation density.

the PtOEP, PtOEP triplets are formed very efficiently, and then undergo energy transfer[63] to form the lower energy DRCN5T triplets. If the 1100 nm TA band is due to DRCN5T triplets—as we have hypothesized—then its amplitude should increase due to the added contribution to its population via the sensitization. Since we cannot selectively excite the PtOEP, the long-range heavy atom effect may also contribute.[64,65] As shown in Figure S12, Supporting Information, this is exactly what we observe. As we increase the percentage weighting of PtOEP in the DRCN5T:PtOEP blend, the sensitization process becomes more efficient and a progressive increase in the signal amplitude of the 1100 nm band is observed. This is therefore entirely consistent with the assignment of the 1100 nm band to DRCN5T triplets, and denotes an increase in the DRCN5T triplet population relative to the pristine DRCN5T film due to the sensitization. Note that this enhancement of the 1100 nm band cannot be attributed to the PtOEP triplet. We assessed this by examining a PtOEP:polystyrene blend with the maximum PtOEP weighting of 50%, and the PtOEP triplet occurs below 900 nm, with a considerably different shape to the one observed in the DRCN5T:PtOEP samples.

Additional evidence for the assignment of the 1100 nm μs-TA band to triplets is a comparison to a previously published dicyanovinyl quinquethiophene,[66] which exhibited a strong triplet absorption at 1025 nm flanked by two polaron transitions: exactly the spectral pattern we observe for DRCN5T:PC70BM. Interestingly, previous spectroscopic work on DRCN5T:PC70BM[43,67] did not uncover the pronounced triplet formation we observe, and this highlights the value of doing TAS on long (μs) timescales and employing oxygen quenching experiments.

The apparent presence of only triplets in the annealed blend TA results is a very unusual observation (Figure 4a). Annealing of DRCN5T:PC70BM devices produces a large increase in the device short-circuit current and hence the consequent power conversion efficiencies rise from 3% to 8%,[31,32] and thus it would be expected that the number of charge carriers observed in the TA results should increase upon annealing. Another unusual observation is that the triplet populations observed in the TAS of the two DRCN5T blends on the microsecond timescale are substantially higher than that seen for the pristine films, by a factor of over two. It should be noted that these measurements were repeated several times to check for reproducibility, and identical trends were achieved each time.

2.5. Picosecond TAS

To gain more insight into these unusual results, ps-TAS (**Figure 5**) was measured for DRCN5T and its PC70BM blends. The normalized spectra are shown in Figure S13, Supporting Information. Figure 5a shows the ps-TAS spectral evolution of unannealed pristine DRCN5T film, where a band centered at 1150 nm with a shoulder at 975 nm at 1 ps quickly decays and is assigned to DRCN5T singlet excitons.[67] At longer times, a new, weak absorption is revealed at 1100 nm, which was assigned to triplets in accordance with the data obtained in μs-TAS.

In the unannealed DRCN5T:PC70BM blend sample (Figure 5b), the DRCN5T singlet exciton at 1150 nm is of lower initial intensity than for the pristine, which is consistent with the singlet exciton quenching seen in the unannealed blend by PL. Similarly to the pristine film, the unannealed blend also showed the triplet band after 1 ns centered at 1100 nm. However, a new species was also observed in the unannealed blend, first appearing at 10 ps with two bands, one at 900 nm and the other one in the region over 1300 nm, both of which rapidly decay over ps-ns timescales. This new set of bands was assigned to polarons, given the similarity to the TA bands remaining on the μs timescales in the unannealed blend.

The annealed DRCN5T:PC70BM blend ps-TAS data shows a singlet exciton band at 1200 nm, a 0.04 eV red-shift compared to unannealed blend and pristine samples (a similar magnitude to the ground state 0-0 transition red-shift of 0.08 eV). As with the ground state absorbance, this red-shift displacement could be due to an enhanced crystallinity of the environment where the exciton is created.[68,69] This is in agreement with previously reported DRCN5T singlet excitons seen in annealed pristine samples.[43,67] In contrast, the triplet band at 1100 nm seen after 1 ns is in the same position as the unannealed blend and pristine samples. Although very weak, the polaron at 1000 nm appears in the annealed blend at 100 ps (more easily seen in the normalized ps-TAS spectra, Figure S13c, Supporting Information). This 1000 nm polaron band is red-shifted compared to the

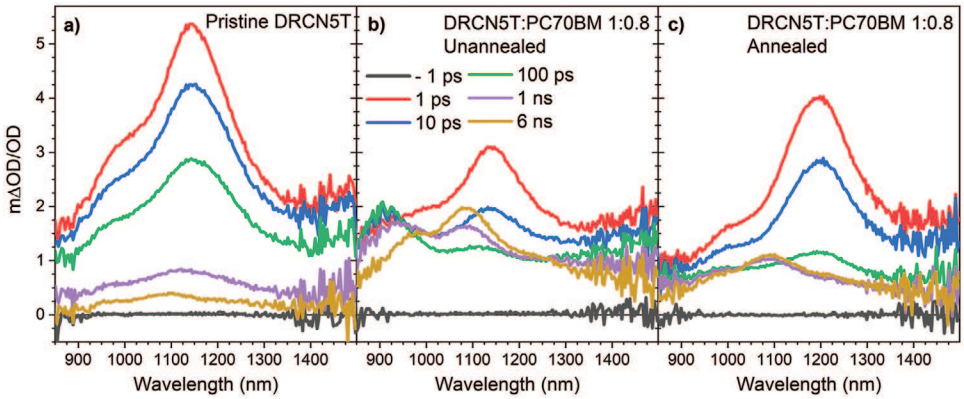

Figure 5. Picosecond transient absorption spectra for a) pristine DRCN5T and b) unannealed and c) annealed DRCN5T:PC70BM (1:0.8) films. Spectra were recorded in a time range from 1 ps to 6 ns, exciting at 510 nm at 12 μJ cm^{-2}.

950 nm polaron band observed for the unannealed blend (in accordance with spectroelectrochemistry experiments reported by Brabec et al[42]). The considerably smaller amplitude of this polaron band upon annealing the blend suggests a much lower population of charge carriers, as observed in the μs-TA data.

Note that the polarons and excitons in the annealed blend were both red-shifted compared to their counterparts in the unannealed blend and pristine film, but the position of the triplet band remains unshifted. The same absorbance spectrum for the triplets suggests that triplets were formed in similar environments in all three samples. This is likely to be a disordered phase, which is common for all three samples (as seen by ground state absorbance and Raman spectra).

To help explain the ps-TAS data, given its complexity and the existence of several different species, global analysis (GA) of the different samples was performed, as shown in **Figure 6**.[70] The pristine DRCN5T sample shows two different species with bands centered at 1100 and 1150 nm, assigned above to triplet and singlet excitons, respectively. GA of the unannealed DRCN5T:PC70BM sample shows these same two bands, but also a new species which absorbs at 900 nm and from 1200 nm into the NIR. This absorbance profile is very similar to both the calculated DRCN5T polaron absorbance (Figure S10, Supporting Information) and the μs-TA spectrum at long times for the unannealed blend, and thus can be assigned to polarons.

The annealed DRCN5T:PC70BM blend GA shows the presence of two different singlet excitons. The first matches the unannealed pristine and blend samples (a band centered at 1150 nm) and was therefore assigned to excitons originated in more disordered DRCN5T regions. The other exciton band was centered at 1200 nm and assigned to excitons formed in the more crystalline DRCN5T regions. Polarons in the annealed blend sample displayed an absorbance with a band at 900–1000 nm (red-shifted compared to the unannealed blend's polaron, as observed in the μs-TA data) and another band that absorbs from 1200 nm onward.

Figure 6 also shows the comparison between the decay dynamics at low fluence (6 μJ cm^{-2}) obtained by GA, with the help of Optimus software,[70] for the singlet exciton, polaron and triplets. Pristine DRCN5T decay dynamics are discussed in Figure S14, Supporting Information. The unannealed blend singlet exciton decays following a multiexponential behavior, again indicating the coexistence of domains with different crystallinity that leads to different relaxation times. However, the singlet exciton is also efficiently quenched via electron transfer in the unannealed blend, given the high amplitude and ultrafast appearance of the DRCN5T polaron band (Figure 5). The polaron decays monoexponentially with a lifetime of 1.5 ns, with little energy density dependence (Figure S15a, Supporting Information), suggesting the presence of geminate recombination: this polaron is a CT state, which is spectrally identical to fully separated polarons. The triplet population is low at early times but rises after 50 ps, reaching a plateau at 2 ns.

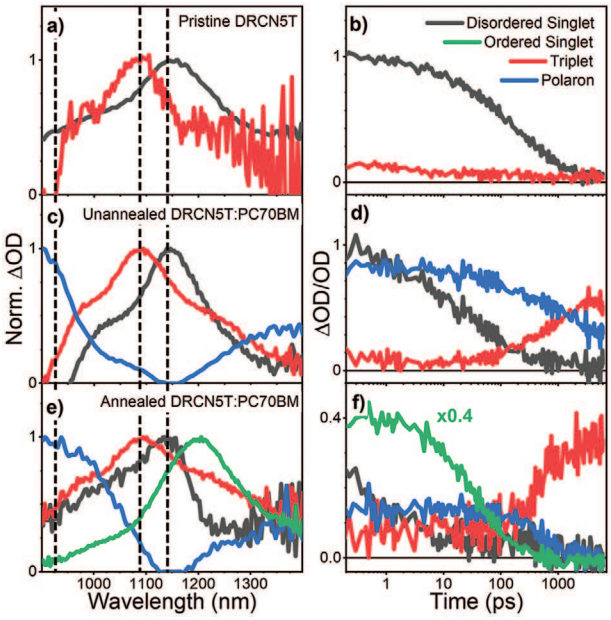

Figure 6. GA data obtained for the a,b) pristine DRCN5T and for the c,d) unannealed and e,f) annealed DRCN5T:PC70BM 1:0.8 blend samples. (a,c,e) show the normalized spectra of the different species obtained by GA. (b,d,f) show the decay obtained by GA of the species in the studied samples. Excitons from the purer domains were labeled as "ordered singlets" in (b) to distinguish them from excitons in disordered regions ("disordered singlets"). The data was obtained exciting at 510 nm with an excitation density of 6 μJ cm^{-2}. The disordered singlet exciton amplitude in (f) was multiplied by 0.4 to enable ease of comparison.

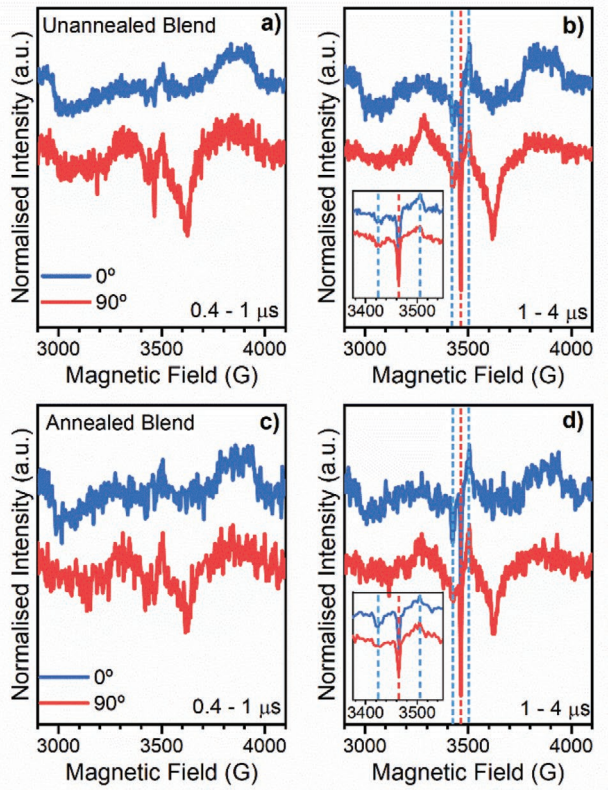

Figure 7. Normalized transient electron paramagnetic resonance (TrEPR) at 290 K of a,b) unannealed and c,d) annealed DRCN5T:PC70BM 1:0.8 films averaged at a,c) 0.4–1 µs and b,d) 1–4 µs measured under two angles 0° (blue trace) and 90° (red trace). Cyan and red vertical lines correspond to peaks associated to PC70BM triplet and DRCN5T charges, respectively.

The relative intensity of the triplet and singlet excitons before 10 ps is similar to the pristine film, indicating that these early triplets are also formed through ISC. However, using the lowest excitation density of 3 µJ cm^{-2}, the rise of the triplet population after 50 ps shows a time constant of 1.5 ns, which matches the polaron decay lifetime of 1.5 ns. This close correspondence and mono-exponential behavior suggest that the late triplet formation is the result of CT state recombination (as seen in the normalized decays, Figure S16a, Supporting Information). CT states are capable of rapid spin-mixing, whereupon the ^{3}CT state can undergo back recombination to the T_1 state. This additional triplet formation mechanism explains the larger triplet TA intensity seen in the unannealed blend compared to the pristine sample in µs-TAS (Figure 4).

The annealed blend GA shows that the disordered and ordered singlet excitons have very different kinetics and relative intensities. The ordered singlet exciton has a much higher relative intensity, indicating a greater presence of this kind of exciton in the annealed sample, as expected given the pronounced crystallinity enhancement and increased domain size after annealing. The disordered excitons decay substantially faster (than the ordered excitons) because they are closer to an amorphous D:A interface, and therefore are preferentially quenched to form charges. In contrast, the ordered excitons decay monoexponentially, indicating a simple return to the ground state: a result of them being localized inside large DRCN5T domains and therefore unable to reach a D:A interface within their lifetime. As a result, the relative population of charges is substantially smaller in the annealed blend. Furthermore, the relative intensities of the disordered singlet exciton and polaron in the annealed sample are very similar to their counterparts in the unannealed blend (Figure 6f). This is further evidence that the ordered singlet excitons in the annealed blend contribute little to charge carrier formation.

Intriguingly, however, the annealed blend polaron shows a similar behavior to that observed in the unannealed blend: a monomolecular decay with $\tau = 1$ ns that matches the rise of the triplet state. Both unannealed and annealed blends achieve similar populations of triplet excitons. It is possible that the slower polaron recombination in the unannealed blend (Figure S16, Supporting Information) compensates for the smaller polaron population in the annealed blend, enabling both blends to reach similar triplet population maxima.

2.6. Electron Paramagnetic Resonance

To examine the triplet and charge states in these blend samples, we performed transient electron paramagnetic resonance (trEPR) experiments (**Figure 7**) at 290 K (to be consistent with the room temperature TAS). The trEPR shows that both blend samples have similar features, namely a DRCN5T triplet state (≈1000 G wide), and a PC70BM triplet state (peaks at ≈3422 G and 3505 G, cyan vertical lines in Figure 7). At later times there is also a charge state signal which is non-Boltzmann populated (centered at $g \approx 2$ at 3465 G, red vertical line). While the exact peak intensities of the DRCN5T triplet in the blend and pristine samples (see Figure S17, Supporting Information, for trEPR on pristine DRCN5T samples) are different, the width and peak positions do match, thereby confirming the broad spectrum in the blend to be that of the DRCN5T triplet state. Interestingly, the pristine DRCN5T also shows some evidence of a charged state.

The early time spectra (0.4–1 µs) for both the unannealed and annealed blend samples show a DRCN5T triplet spectrum which is consistent with an ISC mechanism. At later time intervals of 1–2 µs, the DRCN5T triplet polarisation pattern is harder to ascribe as being either eea/eaa or eaa/eaa (which would be consistent with an ISC or recombination triplet, respectively). Furthermore, the weak trEPR signal at room temperature means only time averaged signals can show clear spectra and this makes observation of the evolution of the triplet harder. However, the radical or charge signal at 3465 G is non-Boltzmann populated and therefore this could be indicative of a CT state. As such, a recombination triplet may indeed be present. A full EPR study is ongoing, the results of which will be the subject of a future publication. Regardless, the trEPR is in agreement with the TA data, as both show the simultaneous existence of triplet and charge states in the blends. We do not directly observe PC70BM triplets in the TA data, but this could be because their absorption cross-section is much lower than the DRCN5T. The full trEPR analysis discussion, including the orientation effect, as well as the trEPR of the pristine samples, is in the SI (Figure S17, Supporting Information).

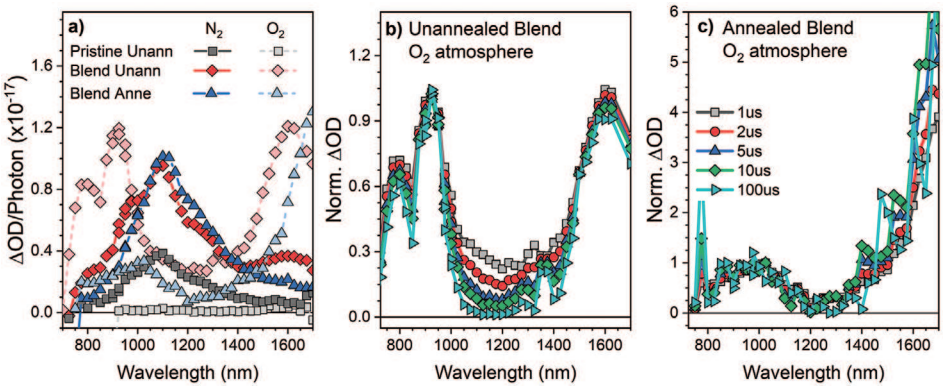

Figure 8. a) TA spectra obtained at 1 µs for the unannealed pristine DRCN5T (black squares), and the unannealed (red diamonds) and annealed (blue triangles) DRCN5T:PC70BM 1:0.8 blend under nitrogen (solid line and darker color symbols) and oxygen (dashed line and lighter color symbols) atmospheres. These spectra were normalized per photon absorbed. Normalized TA spectra recorded over a time range from 1 to 100 µs for b) unannealed and c) annealed blend samples under oxygen atmosphere. Spectra were recorded with a pump wavelength of 500 nm, at 10–15 µJ cm^{-2} excitation density.

2.7. Effects of Oxygen

An intriguing aspect of the DRCN5T blend was the effect of oxygen, particularly in the µs-TAS. The disappearance of the triplet was not the only phenomenon occurring when these samples were measured under oxygen conditions. Typically, oxygen causes only a reversible quenching of the triplet signal population. In the case of DRCN5T:PC70BM blends, however, there was a considerable enhancement in the polaron's TA intensity (by a factor of greater than four at 1600 nm), as seen in **Figure 8**a. For the unannealed blend sample, the oxygen atmosphere led to the disappearance of the 1100 nm triplet band and the sole presence of the bands assigned to DRCN5T polarons. The 1000–1400 nm region (where the triplet absorbs) decays rapidly (Figure 8b), which is in accordance with the fast oxygen quenching of the triplet.[71,72]

A similar phenomenon occurs in the annealed blend sample. The µs TA spectrum recorded under oxygen atmosphere has a similar profile to the polaron bands seen in the ps-TAS GA data (Figure 6). However, unlike the unannealed blend, these two µs bands in the annealed blend show slightly different kinetics (as displayed by the spectral evolution shown in Figure 8c), suggesting the presence of an additional spectral component not previously observable due to the dominance of the DRCN5T triplet. Note that the 1000 nm band is in the same spectral region as PC70BM triplets.[73] However, this assignment is unlikely as both PC60BM and PC70BM blends show identical spectra under oxygen, negating the presence of the PC70BM triplet (Figure S18, Supporting Information). The two different DRCN5T species seen in the annealed spectrum under oxygen could be attributed to polarons in domains with different crystallinity, as shown before in literature for different OPV materials, and consistent with the presence of both crystalline and amorphous regions showed by the Raman spectroscopy.[74,75] Furthermore, faster kinetics are often associated with polarons in more amorphous domains, where the positive polaron has more accessibility to the fullerene anion. In contrast, slower kinetics are assigned to polarons localized/trapped in more crystalline, and thus lower energy, domains.[76] The band centered at 1700 nm may thus correspond to DRCN5T polarons localized in more crystalline regions while the band at 1000 nm corresponds to polaron in more amorphous domains with greater D/A interfacial area. This is consistent with the change in relative intensities of the 1000 and 1700 nm polaron bands upon annealing under oxygen, with the annealed blend showing a greater proportion of polarons in crystalline regions.

It was observed that the presence of oxygen enhances the polaron lifetime as well as the population in the two blends on these µs timescales. (Figure S19, Supporting Information). The TA signal decays under oxygen following a power law, which is typically expected for polarons in OPV blends.[77] One feasible explanation for this enhancement is the existence of a triplet-charge annihilation (TCA) process in these blends.[73,78–81] Triplets enable TCA under inert atmosphere, thereby lowering the polaron population. The oxygen atmosphere quenches the triplets and thus allows the intrinsic polaron population and kinetics to be observed. The photophysical processes in DRCN5T blends with and without the presence of oxygen are summarised in **Scheme 1**.

The timescale of the TCA process is likely to be on the early nanosecond timescales. Figure S20, Supporting Information, shows the raw excitation density dependence of the ps-TA signal recorded at 1100 nm, matching the DRCN5T triplet maximum absorbance, for the unannealed and annealed blends. The triplet population reaches its maximum at earlier times with greater excitation densities. This is in accordance with a second order process such as TCA: the greater the excitation density, the higher the triplet and polaron populations and, therefore, the faster they can react together and begin reducing the population. Moreover, the relative triplet population at 6 ns is lower for higher excitation densities, which also implies a second order triplet annihilation process (TCA in our case). Interestingly, more efficient TCA is observed for the annealed blend, likely due to the higher crystallinity and, therefore, higher charge mobility. Critically, this high charge mobility may enable charges to be extracted before triplets can have a significant impact in device performance.[82]

3. Discussion

The very low charge carrier population observed in annealed DRCN5T:PC70BM blends seems contradictory to literature

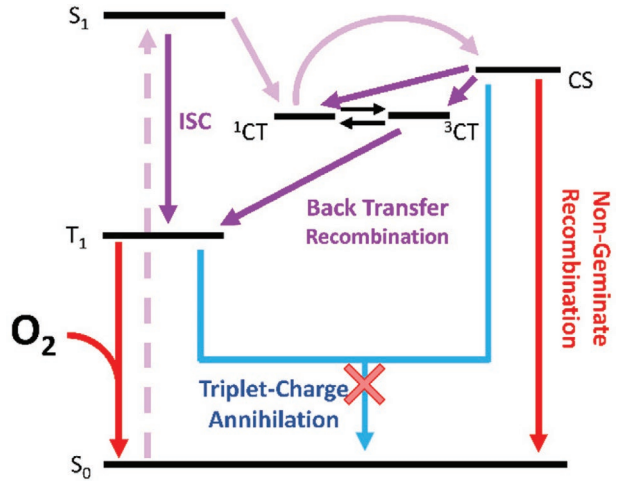

Scheme 1. Summary of the processes occurring in DRCN5T blend systems under inert atmosphere (blue arrows) and under oxygen (red arrows and red cross). Purple arrows illustrate the processes that take place both under inert and oxygen atmospheres.

device efficiency reports. However, it should be noted that other factors play an important role: as mentioned above, charge carrier mobility in DRCN5T blends is enhanced significantly upon annealing, and thus what few charges are created will be extracted very efficiently.[83] Furthermore, the observations that the PL increases significantly in the pristine DRCN5T sample upon annealing in addition to the high population of ordered singlet excitons indicate that photon recycling could be a vital contributor to the enhanced performance. If an ordered singlet exciton does relax radiatively, the emitted photon can be reabsorbed to contribute to device efficiency, but this would not be recorded by TAS, which is a single-pulse technique. This hypothesis would also explain the high PL quenching observed for the annealed pristine/blend samples (Figure 1): standard PL is a steady-state technique and thus the accumulative effect of photon recycling would be included in this measurement. Photon recycling relies on the overlap between the absorption and emission spectra of the material in question. It is important to note that while the overlap for unannealed DRCN5T is very small, we estimate that it increases significantly by a factor of six upon annealing due to the large absorbance red-shift (Figure S21, Supporting Information). This is consistent with our hypothesis that photon recycling is a contributor to device performance for annealed DRCN5T:PC70BM.

The higher TCA efficiency observed for the annealed DRCN5T:PC70BM blend is likely another contributing factor accounting for the low polaron populations in the µs-TA annealed blend spectrum. Such strong TCA was an unexpected observation and is often not considered as a possible loss mechanism in OPV blends. As such, to prove the generality of the TCA process taking place in DRCN5T blends, we blended DRCN5T with two different NFAs: Y6 and ITIC. Figure S22, Supporting Information, shows the comparison of the DRCN5T:PC70BM blend TA spectrum under nitrogen and oxygen with the spectra of the NFA blends. In both cases, the NFA blends under nitrogen lead to a similar spectrum to the PC70BM blend spectrum obtained under nitrogen: a triplet band centered at 1100 nm. Interestingly the DRCN5T:Y6 blend showed a higher intensity on the shoulder centered at 1000 nm that was not present in the other blends. This increase in the TA signal was identified as the contribution of the Y6 negative polaron.[84] In both cases the spectrum radically changed under oxygen, showing the DRCN5T polaron bands at 900 and 1600 nm, confirming the presence of TCA. This is an important observation, as it suggests TCA could be an issue for non-fullerene blends as well as fullerene blends, and thus should be considered when addressing loss mechanisms in new systems.

These experiments with different NFAs, along with the ones performed with PC70BM and PC60BM, validates the TAS measurements under oxygen as a valuable method to prove the existence of the TCA process and to study them in OPV materials. While DRCN5T:PC70BM's stability under oxygen makes it an excellent candidate to assess the role of TCA, our proposed methodology to check for the existence of TCA in other OPV blends is likely still feasible. Oxygen quenching experiments are standard procedures in µs-TAS and have been applied successfully to many conjugated polymer systems.[5,74,85] The short oxygen exposure times in such experiments usually preclude oxygen-induced degradation. The key to successful use of our TCA methodology is therefore an assessment of the reversibility of the reaction (Figure S7, Supporting Information): any oxygen-induced degradation will prevent a full reversibility.

Indeed, another intriguing observation in the DRCN5T:PC70BM blends is the pronounced triplet formation: unusual for such a high efficiency blend. The presence of triplets in DRCN5T is consistent with triplets seen in structurally similar dicyanovinyl quinquethiophenes (DCV5Ts).[66,86] These DCV5T molecules share the same oligothiophene backbone as well as the dicyanovinyl as terminal groups, however they lack the oxothiazolidine groups of DRCN5T. DCV5Ts show similar photophysical and electronic properties to DRCN5T, both possessing similar triplet and polaron spectral features and identical HOMO/LUMO energy values. However, these DCV5Ts showed comparable triplet generation rates between the pristine material and the blend: this is in stark contrast to DRCN5T, which has significantly greater triplet generation in the blend, a result of the pronounced charge recombination. According to the DFT calculations of DRCN5T in Figure S2, Supporting Information, the dihedral angle between each oxothiazolidine group and the terminal thiophene is zero irrespective of whether the conformer is distorted or planar (i.e., the main distortion occurs between the central thiophene rings). This is consistent with the Raman characterization (Figure S3, Supporting Information): the bands assigned to the oxothiazolidine terminal group do not vary largely upon annealing. The implication of this observation is that the introduction of the oxothiazolidine groups enables a greater planarisation of the DRCN5T molecule relative to DCV5T. This may enable a closer alignment between the π-systems of donor and acceptor, facilitating the back recombination to form the DRCN5T triplet.

A further point of interest lies in the annealing of the material. Ziehlke et al. demonstrated that heating the substrate prior to active layer deposition resulted in fewer triplets and more polarons for DCV5T, but this was also accompanied by a loss of crystallinity.[66] While their methodology is not identical to

our thermal annealing, similar principles apply. In contrast, therefore, DRCN5T exhibits significant improvements in crystallinity upon heating (annealing). In addition to the oxothiazolidine promoting greater planarisation, it is also noteworthy that the alkyl chain lengths of DRCN5T are octyl groups, rather than the butyls used in DCV5T. The longer alkyl chain lengths could allow for interdigitation and thus enhanced crystallinity upon annealing.[87–89]

This work points out the urgent need of using new strategies to suppress triplet formation and thus preclude TCA. Several approaches can be undertaken to achieve this. One strategy could be the employment of triplet scavengers to annihilate the triplets formed and negate the effect of TCA. Other approaches in the literature include incorporation of a delayed fluorescence emitter as a ternary component[90] and fluorination of a material to increase the triplet energy level and thus hinder the triplet CT state to local triplet transition.[91] However, this approach has led to similar solar cell efficiencies for DRCN5T and 2F-DRCN5T.[33] Moreover, our work in this paper concludes that DRCN5T triplets are formed in amorphous regions; another approach could be to fabricate materials where the polaron formation is favored in more crystalline domains, thus spatially separating polarons from the triplets. It has been shown that certain materials have the ability to form polarons in both crystalline and amorphous regions, showing two different polaron absorbance features.[74,75] For this particular approach, the energy sink phenomenon may play an important role: polarons, once formed, may be rapidly transferred to more crystalline domains.[92,93]

4. Conclusions

The small molecule DRCN5T, an electron donor for OPV, has been investigated with a combination of morphological and spectroscopic techniques, and blended with a variety of fullerene and NFAs. Extensive enhancements in crystallinity are observed upon annealing. Unusually for such a high efficiency blend, however, a high triplet population is observed. These triplets are primarily formed in the amorphous regions via back recombination from a CT state.

The presence of triplets in DRCN5T is detrimental for device efficiency for two reasons. The formation of triplets from a CT state rather than the desired charge carriers represents a loss pathway. Moreover, we also show that these triplets are responsible for a substantial decrease in charge population through TCA. However, literature OPV device efficiencies for annealed DRCN5T:PC70BM show that high efficiencies can be achieved, despite the significant presence of triplets observed. We have shown that this is not due to greater charge photogeneration upon annealing. The large, crystalline, pure domains of DRCN5T that form after annealing inhibit excitons photogenerated in these regions from being dissociated within their lifetime, leading to a decrease in charge carrier generation. Instead, it is the enhancement in PL upon annealing that likely enables photon recycling under device conditions, in addition to greater charge carrier mobilities, that increases device efficiencies.

Importantly, we also demonstrate the generality of the TCA in a variety of DRCN5T:acceptor blends. TCA is typically inferred rather than directly observed, and thus we conclude that μs-TAS under oxygen conditions is a reliable method to demonstrate the existence of TCA. The above points emphasize the need for high PL quantum yields and inhibited triplet formation for the OPV field to reach the 20% efficiency landmark.

5. Experimental Section

Materials and Sample Fabrication: 99% purity DRCN5T, Y6, and ITIC were purchased from Ossila and PC60BM and PC70BM from Solenne. Blend films were prepared via spin-coating 20 mg mL^{-1} DRCN5T:acceptor 1:0.8 (by weight) in chloroform (anhydrous, Sigma Aldrich) solution at 2000 rpm under nitrogen atmosphere. Pristine samples were prepared from a 15 mg mL^{-1} DRCN5T in chloroform solution instead. Film samples were fabricated following literature procedures exactly in order to replicate the active layers found in high efficiency devices. However, as is standard for TAS experiments, samples were fabricated without electrodes and, therefore, samples were measured under open-circuit conditions (charges were not extracted).

Samples for sensitization experiments were prepared in similar fashion to pristine DRCN5T materials: preparing a 15 mg mL^{-1} in chloroform solutions with the corresponding PtOEP ratio (10%, 25%, and 50%) and spin-coated at 2000 room under nitrogen atmosphere. PSS:PtOEP reference film was prepared spin-coating a 15 mg mL^{-1} (1:1 in weight) solution in chloroform at 2000 rpm.

Characterization: Ground state absorbance was obtained with a Perkin Elmer Lambda 365. PL was measured in a Horiba Jobin-Yvon Fluorolog-3.

Grazing Incidence Small Angle X-Ray Scattering: Grazing incidence small angle X-ray scattering and GIWAXS were performed on the Xuess instrument equipped with an Excillum MetalJet liquid gallium X-ray source. Alignment was performed on silicon substrates via three iterative height (z) and rocking curve (Ω) scans, with the final grazing incidence angle set to $\Omega = 0.3°$. Scattering patterns were recorded on a vertically-offset Pilatus 1M detector with a sample to detector distance of 307 mm, calibrated using a silver behenate standard to achieve a q-range of 0.1–2.0 $Å^{-1}$. 2D images were recorded with exposure times of 600 s. Data correction and reduction were performed using the GIXSGUI MATLAB toolbox.[94] 2D scattering data was reshaped and reduced to 1D via radial integration, which was performed with a mask to remove contributions from "hot pixels," the substrate horizon, and the reflected beam.

Raman Spectroscopy: Raman spectra were recorded using a custom-made back scattering setup with an Andor iDus 416 CCD camera attached to an Andor Shamrock 500i spectrograph. Raman signal was generated via excitation with a 6 ns, 10 Hz Nd:YAG laser (Spectra-Physics, INDI-40-10) for the excitation pulse. The intensity of the Raman excitation was decreased with the use of neutral density filters to maintain it at 0.1 mW, measured with an ES111C sensor (Thorlabs). The excitation wavelength was selected with a versaScan L-532 OPO and the appropriate notch filters were used in front of the spectrograph slits (200 mm).

Raman spectra in Figure 3a were measured with a Renishaw inVia Raman microscope in a backscattering configuration. Samples were placed in a Linkam (THMS600) stage that provided an inert atmosphere. 457 nm excitation was obtained with an argon-ion laser (ModuLaser) using low power (<0.1 mW), with acquisition time of around 30 s, and defocussed laser (≈10 μm spot). The spectral resolution was ± 0.7 cm^{-1}.

Microsecond TAS: Microsecond TAS was recorded using a 6 ns, 10 Hz Nd:YAG laser (Spectra-Physics, INDI-40-10) for the excitation pulse. The excitation wavelength was selected with a versaScan L-532 OPO. Excitation density was set from 3 to 200 μJ cm^{-2} using neutral density

filters, and measured with an ES111C sensor (Thorlabs). Probe light was provided by a quartz tungsten halogen lamp (IL1, Bentham). The TA signals were recorded with Si and InGaAs photodiodes coupled to a preamplifier and an electronic filter (Costronic Electronics) connected to a Tektronix DPO4034B oscilloscope and PC. Probe wavelengths were selected with a Cornerstone 130 monochromator (Oriel Instruments) before the detector. During measurements films were kept in a sealed cuvette connected to either nitrogen or oxygen flow.

Picosecond TAS: Ultrafast TAS was conducted on the femtosecond to nanosecond timescale using a regeneratively amplified Ti:sapphire laser system (Solstice, Spectra-Physics) and Helios spectrometers (Ultrafast Systems), which generated 800 nm laser pulses (pulse width: 92 fs, repetition rate: 1 kHz). To generate the pump, a fraction of the 800 nm beam was directed through a sequence of optical parametric amplifiers (TOPAS Prime, Spectra-Physics) and a frequency mixer (NIR/UV-Vis, Light Conversion) to tune the excitation wavelength to 355 nm. The intensity of the pump was modulated using neutral density filters, and measured using an energy meter (VEGA, P/N 7Z01560, OPHIR Photonics), fitted with a 0.5 mm diameter aperture. The pump beam at the sample was ≥0.5 mm. A visible white light continuum (WLC) was used as the probe, generated from a fraction of the 800 nm pulse, focused onto a Ti:sapphire crystal. The probe beam was delayed with respect to the pump beam using a motorized delay stage to alter the path length of the probe beam before generation of the WLC. To reduce the noise, the WLC was split into two beams, one of which was passed through the sample, and the other used as a reference. Both beams were subsequently focused onto separate fiber-optic coupled, multichannel spectrometers (CMOS sensors). Alternate pump pulses were blocked using a synchronized chopper (500 Hz). As such, absorption spectra of the excited and unexcited sample were obtained to determine the time-resolved absorption difference spectrum. Time zero was then adjusted to match the rise of the signal at each wavelength.

trEPR: EPR was measured on samples deposited on quartz substrates flame sealed in 4.9 mm quartz EPR tubes, under vacuum (8×10^{-5}–10^{-4} mbar) and fixed inside the tube by Teflon tape. A 532 nm pulsed laser (1 mJ, 5 ns pulse length, 100 Hz repetition rate) was used to excite the sample in combination with a depolarizer to avoid polarization effects. The transient EPR experiments were performed on a laboratory-built X-band (9.7 GHz) continuous wave spectrometer together with a Bruker MD5 resonator with optical access.[95] The temperature was controlled using a temperature controller and Helium flow cryostat, samples were measured at 290 K. Angle dependent transient EPR studies were carried out with the use of a goniometer. Samples were measured at two angles, ≈0° and 90°, where 0° was when the incident laser excitation was parallel to the substrate normal and the magnetic field direction was parallel to the substrate plane and where 90° was when the incident laser excitation was parallel to the substrate plane and the magnetic field direction was parallel to the substrate normal.

Supporting Information

Supporting Information is available from the Wiley Online Library or from the author.

Acknowledgements

The authors acknowledge the Optoelectronics Group at the University of Cambridge for sharing the software for global analysis and the James Durrant group at Imperial College London for use of their ps-TAS instrument. T.M.C. would like to acknowledge support from EPSRC project EP/N026411/1. S.L. and J.S.K. thank the UK EPSRC ATIP Programme Grant (EP/T028513/1) and the Global Research Laboratory Program of the Korean National Research Foundation (NRF) funded by the Ministry of Science, ICT & Future Planning (NRF-2017K1A1A2 013153).

Conflict of Interest

The authors declare no conflict of interest.

Data Availability Statement

The data that support the findings of this study are available from the corresponding author upon reasonable request.

Keywords

DRCN5T, non-fullerene acceptors, Raman, spectroscopy, transient absorption spectroscopy, triplets

Received: February 15, 2021
Revised: April 15, 2021
Published online:

[1] Q. Liu, Y. Jiang, K. Jin, J. Qin, J. Xu, W. Li, J. Xiong, J. Liu, Z. Xiao, K. Sun, S. Yang, X. Zhang, L. Ding, *Sci. Bull.* **2020**, *65*, 272.
[2] Y. Lin, M. I. Nugraha, Y. Firdaus, A. D. Scaccabarozzi, F. Aniés, A.-H. Emwas, E. Yengel, X. Zheng, J. Liu, W. Wahyudi, E. Yarali, H. Faber, O. M. Bakr, L. Tsetseris, M. Heeney, T. D. Anthopoulos, *ACS Energy Lett.* **2020**, *12*, 3663.
[3] J. J. Benson-Smith, H. Ohkita, S. Cook, J. R. Durrant, D. D. C. Bradley, J. Nelson, *Dalton Trans.* **2009**, 10000, https://doi.org/10.1039/B910675H.
[4] D. Veldman, S. C. J. Meskers, R. A. J. Janssen, *Adv. Funct. Mater.* **2009**, *19*, 1939.
[5] C. Dyer-Smith, L. X. Reynolds, A. Bruno, D. D. C. Bradley, S. A. Haque, J. Nelson, *Adv. Funct. Mater.* **2010**, *20*, 2701.
[6] A. Riaño, P. Mayorga Burrezo, M. J. Mancheño, A. Timalsina, J. Smith, A. Facchetti, T. J. Marks, J. T. López Navarrete, J. L. Segura, J. Casado, R. Ponce Ortiz, *J. Mater. Chem. C* **2014**, *2*, 6376.
[7] A. J. Gillett, A. Privitera, R. Dilmurat, A. Karki, D. Qian, A. Pershin, G. Londi, W. K. Myers, J. Lee, J. Yuan, S.-J. Ko, M. K. Riede, F. Gao, G. C. Bazan, A. Rao, T.-Q. Nguyen, D. Beljonne, R. H. Friend, arXiv preprint *arXiv:2010.10978,* **2020**.
[8] S. D. Dimitrov, J. R. Durrant, *Chem. Mater.* **2014**, *26*, 616.
[9] Y. Xu, H. Yao, L. Ma, J. Wang, J. Hou, *Rep. Prog. Phys.* **2020**, *83*, 082601.
[10] S. D. Dimitrov, S. Wheeler, D. Niedzialek, B. C. Schroeder, H. Utzat, J. M. Frost, J. Yao, A. Gillett, P. S. Tuladhar, I. McCulloch, J. Nelson, J. R. Durrant, *Nat. Commun.* **2015**, *6*, 6501.
[11] B. Hu, L. Yan, M. Shao, *Adv. Mater.* **2009**, *21*, 1500.
[12] A. Rao, P. C. Y. Chow, S. Gélinas, C. W. Schlenker, C. Li, H. Yip, A. K.-Y. Jen, D. S. Ginger, R. H. Friend, *Nature* **2013**, *500*, 435.
[13] S. Westenhoff, I. A. Howard, J. M. Hodgkiss, K. R. Kirov, H. A. Bronstein, C. K. Williams, N. C. Greenham, R. H. Friend, *J. Am. Chem. Soc.* **2008**, *130*, 13653.
[14] E. Salvadori, N. Luke, J. Shaikh, A. Leventis, H. Bronstein, C. W. M. Kay, T. M. Clarke, *J. Mater. Chem. A* **2017**, *5*, 24335.
[15] X.-K. Chen, T. Wang, J.-L. Brédas, *Adv. Energy Mater.* **2017**, *7*, 1602713.
[16] F. Kraffert, R. Steyrleuthner, S. Albrecht, D. Neher, M. C. Scharber, R. Bittl, J. Behrends, *J. Phys. Chem. C* **2014**, *118*, 28482.
[17] S. M. Menke, A. Sadhanala, M. Nikolka, N. A. Ran, M. K. Ravva, S. Abdel-Azeim, H. L. Stern, M. Wang, H. Sirringhaus, T.-Q. Nguyen, J.-L. Brédas, G. C. Bazan, R. H. Friend, *ACS Nano* **2016**, *10*, 10736.
[18] L. Xue, Y. Yang, J. Xu, C. Zhang, H. Bin, Z.-G. Zhang, B. Qiu, X. Li, C. Sun, L. Gao, J. Yao, X. Chen, Y. Yang, M. Xiao, Y. Li, *Adv. Mater.* **2017**, *29*, 1703344.

[19] C. W. Schlenker, K.-S. Chen, H.-L. Yip, C.-Z. Li, L. R. Bradshaw, S. T. Ochsenbein, F. Ding, X. S. Li, D. R. Gamelin, A. K.-Y. Jen, D. S. Ginger, *J. Am. Chem. Soc.* **2012**, *134*, 19661.
[20] L. Yang, W. Gu, L. Lv, Y. Chen, Y. Yang, P. Ye, J. Wu, L. Hong, A. Peng, H. Huang, *Angew. Chem., Int. Ed.* **2018**, *57*, 1096.
[21] X. Gao, Y. Liang, H. Wang, T. Yang, S. Huettner, J. Wang, F. Zhu, Y. Tao, *Org. Electron.* **2019**, *70*, 93.
[22] B. T. Luppi, D. Majak, M. Gupta, E. Rivard, K. Shankar, *J. Mater. Chem. A* **2019**, *7*, 2445.
[23] Q. Wu, Y. Cheng, Z. Xue, X. Gao, M. Wang, W. Yuan, S. Huettner, S. Wan, X. Cao, Y. Tao, W. Huang, *Chem. Commun.* **2019**, *55*, 2640.
[24] H. Zhen, Q. Hou, K. Li, Z. Ma, S. Fabiano, F. Gao, F. Zhang, *J. Mater. Chem. A* **2014**, *2*, 12390.
[25] Y. Shao, Y. Yang, *Adv. Mater.* **2005**, *17*, 2841.
[26] T. B. Fleetham, Z. Wang, J. Li, *Inorg. Chem.* **2013**, *52*, 7338.
[27] N. Wang, J. Yu, Y. Zheng, Z. Guan, Y. Jiang, *J. Phys. Chem. C* **2012**, *116*, 5887.
[28] D. W. Gehrig, I. A. Howard, F. Laquai, *J. Phys. Chem. C* **2015**, *119*, 13509.
[29] T. M. Clarke, A. Ballantyne, S. Shoaee, Y. W. Soon, W. Duffy, M. Heeney, I. McCulloch, J. Nelson, J. R. Durrant, *Adv. Mater.* **2010**, *22*, 5287.
[30] H. Cha, C.-H. Tan, J. Wu, Y. Dong, W. Zhang, H. Chen, S. Rajaram, K. S. Narayan, I. McCulloch, J. R. Durrant, *Adv. Energy Mater.* **2018**, *8*, 1801537.
[31] M. Zhang, F. Zhang, Q. An, Q. Sun, W. Wang, X. Ma, J. Zhang, W. Tang, *J. Mater. Chem. A* **2017**, *5*, 3589.
[32] B. Kan, M. Li, Q. Zhang, F. Liu, X. Wan, Y. Wang, W. Ni, G. Long, X. Yang, H. Feng, Y. Zuo, M. Zhang, F. Huang, Y. Cao, T. P. Russell, Y. Chen, *J. Am. Chem. Soc.* **2015**, *137*, 3886.
[33] M. Babics, T. Duan, A. H. Balawi, R.-Z. Liang, F. Cruciani, I.-D. Carja, D. Gottlieb, I. McCulloch, K. Vandewal, F. Laquai, P. M. Beaujuge, *ACS Appl. Energy Mater.* **2019**, *2*, 2717.
[34] J. Huang, X. Zhang, D. Zheng, K. Yan, C.-Z. Li, J. Yu, *Sol. RRL* **2017**, *1*, 1600008.
[35] J. Zhao, Y. Li, G. Yang, K. Jiang, H. Lin, H. Ade, W. Ma, H. Yan, *Nat. Energy* **2016**, *1*, 15027.
[36] Y. Wang, Y. Wang, B. Kan, X. Ke, X. Wan, C. Li, Y. Chen, *Adv. Energy Mater.* **2018**, *8*, 1802021.
[37] K.-N. Zhang, X.-Y. Yang, M.-S. Niu, Z.-C. Wen, Z.-H. Chen, L. Feng, X.-J. Feng, X.-T. Hao, *Org. Electron.* **2019**, *66*, 13.
[38] L. Zhang, N. Yi, W. Zhou, Z. Yu, F. Liu, Y. Chen, *Adv. Sci.* **2019**, *6*, 1900565.
[39] Q. An, F. Zhang, X. Yin, Q. Sun, M. Zhang, J. Zhang, W. Tang, Z. Deng, *Nano Energy* **2016**, *30*, 276.
[40] K. Zhang, J. Guo, L. Zhang, C. Qin, H. Yin, X. Gao, X. Hao, *Adv. Funct. Mater.* **2021**, 2100316, https://doi.org/10.1002/adfm.202100316.
[41] M. N. Uvarov, M. S. Plekhanov, V. A. Zinoviev, V. V. Yanshole, M. V. Fedin, L. V. Kulik, *Chem. Phys. Lett.* **2020**, *754*, 137647.
[42] J. Min, X. Jiao, V. Sgobba, B. Kan, T. Heumüller, S. Rechberger, E. Spiecker, D. M. Guldi, X. Wan, Y. Chen, H. Ade, C. J. Brabec, *Nano Energy* **2016**, *28*, 241.
[43] A. Weu, R. Kumar, J. F. Butscher, V. Lami, F. Paulus, A. A. Bakulin, Y. Yaynzof, *Adv. Funct. Mater.* **2020**, *30*, 1907432.
[44] J. Min, N. S. Güldal, J. Guo, C. Fang, X. Jiao, H. Hu, T. Heumüller, H. Ade, C. J. Brabec, *J. Mater. Chem. A* **2017**, *5*, 18101.
[45] T. Erb, U. Zhokhavets, G. Gobsch, S. Raleva, B. Stühn, P. Schilinsky, C. Waldauf, C. J. Brabec, *Adv. Funct. Mater.* **2005**, *15*, 1193.
[46] N. Cho, K. Song, J. K. Lee, J. Ko, *Chem. - Eur. J.* **2012**, *18*, 11433.
[47] J. K. Lee, B.-S. Jeong, J. Kim, C. Kim, J. Ko, *J. Photochem. Photobiol., A* **2013**, *251*, 25.
[48] M. Berlinghof, S. Langner, C. Harreiß, E. M. Schmidt, R. Siris, F. Bertram, C. Shen, J. Will, T. Schindler, A. Prihoda, S. Rechberger, G. S. Duesberg, R. B. Neder, E. Spiecker, C. J. Brabec, T. Unruh, *Z. Kristallogr.- Cryst. Mater.* **2020**, *235*, 15.
[49] X. Rodríguez-Martínez, M. S. Vezie, X. Shi, I. McCulloch, J. Nelson, A. R. Goñi, M. Campoy-Quiles, *J. Mater. Chem. C* **2017**, *5*, 7270.
[50] S. Garreau, M. Leclerc, N. Errien, G. Louarn, *Macromolecules* **2003**, *36*, 692.
[51] J. Casado, R. Réau, J. T. López Navarrete, *Chem. - Eur. J.* **2006**, *12*, 3759.
[52] W. C. Tsoi, D. T. James, J. S. Kim, P. G. Nicholson, C. E. Murphy, D. D. C. Bradley, J. Nelson, J.-S. Kim, *J. Am. Chem. Soc.* **2011**, *133*, 9834.
[53] J. Casado, V. Hernández, S. Hotta, J. T. L. Navarrete, *Adv. Mater.* **1998**, *10*, 1458.
[54] D. P. Strommen, K. Nakamoto, *J. Chem. Educ.* **1977**, *54*, 474.
[55] R. Loudon, *J. Phys.* **1965**, *26*, 677.
[56] S. Hu, K. M. Smith, T. G. Spiro, *J. Am. Chem. Soc.* **1996**, *118*, 12638.
[57] S. Wood, J. R. Hollis, J.-S. Kim, *J. Phys. D: Appl. Phys.* **2017**, *50*, 073001.
[58] J. L. Donnelly, D. Offenbartl-Stiegert, J. M. Marín-Beloqui, L. Rizzello, G. Battaglia, T. M. Clarke, S. Howorka, J. D. Wilden, *Chem. - Eur. J.* **2020**, *26*, 863.
[59] Y. Li, T. Pullerits, M. Zhao, M. Sun, *J. Phys. Chem. C* **2011**, *115*, 21865.
[60] J. Ku, Y. Lansac, Y. H. Jang, *J. Phys. Chem. C* **2011**, *115*, 21508.
[61] S. Kahmann, D. Fazzi, G. J. Matt, W. Thiel, M. A. Loi, C. J. Brabec, *J. Phys. Chem. Lett.* **2016**, *7*, 4438.
[62] S. Ghosh, V. Gueskine, M. Berggren, I. V. Zozoulenko, *J. Phys. Chem. C* **2019**, *123*, 15467.
[63] F. Etzold, I. A. Howard, N. Forler, A. Melnyk, D. Andrienko, M. R. Hansen, F. Laquai‡, *Energy Environ. Sci.* **2015**, *8*, 1511.
[64] C. Rothe, S. King, A. Monkman, *Nat. Mater.* **2006**, *5*, 463.
[65] Z. S. Romanova, K. Deshayes, P. Piotrowiak, *J. Am. Chem. Soc.* **2001**, *123*, 2444.
[66] H. Ziehlke, L. Burtone, C. Koerner, R. Fitzner, E. Reinold, P. Bäuerle, K. Leo, M. Riede, *Org. Electron.* **2011**, *12*, 2258.
[67] G. Long, B. Wu, A. Solanki, X. Yang, B. Kan, X. Liu, D. Wu, Z. Xu, W. R. Wu, U. S. Jeng, J. Lin, M. Li, Y. Wang, X. Wan, T. C. Sum, Y. Chen, *Adv. Energy Mater.* **2016**, *6*, 1600961.
[68] R. A. Marsh, J. M. Hodgkiss, S. Albert-Seifried, R. H. Friend, *Nano Lett.* **2010**, *10*, 923.
[69] A. K. Ko Kyaw, D. Gehrig, J. Zhang, Y. Huang, G. C. Bazan, F. Laquai, T.-Q. Nguyen, *J. Mater. Chem. A* **2015**, *3*, 1530.
[70] C. Slavov, H. Hartmann, J. Wachtveitl, *Anal. Chem.* **2015**, *87*, 2328.
[71] M. Salvador, N. Gasparini, J. D. Perea, S. H. Paleti, A. Distler, L. N. Inasaridze, P. A. Troshin, L. Lüer, H.-J. Egelhaaf, C. Brabec, *Energy Environ. Sci.* **2017**, *10*, 2005.
[72] Y. W. Soon, S. Shoaee, R. S. Ashraf, H. Bronstein, B. C. Schroeder, W. Zhang, Z. Fei, M. Heeney, I. McCulloch, J. R. Durrant, *Adv. Funct. Mater.* **2014**, *24*, 1474.
[73] P. C. Y. Chow, S. Albert-seifried, S. Gélinas, R. H. Friend, *Adv. Mater.* **2014**, *26*, 4851.
[74] J. M. Marin-Beloqui, K. J. Fallon, H. Bronstein, T. M. Clarke, *J. Phys. Chem. Lett.* **2019**, *10*, 3813.
[75] J. Guo, H. Ohkita, S. Yokoya, H. Benten, S. Ito, *J. Am. Chem. Soc.* **2010**, *132*, 9631.
[76] Y. Tamai, K. Tsuda, H. Ohkita, H. Benten, S. Ito, *Phys. Chem. Chem. Phys.* **2014**, *16*, 20338.
[77] J. Nelson, *Phys. Rev. B* **2003**, *67*, 155209.
[78] A. J. Gesquiere, S.-J. Park, P. F. Barbara, *J. Am. Chem. Soc.* **2005**, *127*, 9556.
[79] Z. Yu, J. Zhang, S. Liu, L. Zhang, Y. Zhao, H. Zhao, W. Xie, *ACS Appl. Mater. Interfaces* **2019**, *11*, 6292.
[80] I. A. Howard, J. M. Hodgkiss, X. Zhang, K. R. Kirov, H. A. Bronstein, C. K. Williams, R. H. Friend, S. Westenhoff, N. C. Greenham, *J. Am. Chem. Soc.* **2010**, *132*, 328.

[81] D. Yuan, L. Niu, Q. Chen, W. Jia, P. Chen, Z. Xiong, *Phys. Chem. Chem. Phys.* **2015**, *17*, 27609.
[82] G. J. Moore, M. Causa', J. F. Martinez Hardigree, S. Karuthedath, I. Ramirez, A. Jungbluth, F. Laquai, M. Riede, N. Banerji, *J. Phys. Chem. Lett.* **2020**, *11*, 5610.
[83] N. Liang, D. Meng, Z. Ma, B. Kan, X. Meng, Z. Zheng, W. Jiang, Y. Li, X. Wan, J. Hou, W. Ma, Y. Chen, Z. Wang, *Adv. Energy Mater.* **2017**, *7*, 1601664.
[84] R. Wang, C. Zhang, Q. Li, Z. Zhang, X. Wang, M. Xiao, *J. Am. Chem. Soc.* **2020**, *142*, 12751.
[85] Y. W. Soon, H. Cho, J. Low, H. Bronstein, I. McCulloch, J. R. Durrant, *Chem. Commun.* **2013**, *49*, 1291.
[86] K. Schulze, M. Riede, E. Brier, E. Reinold, P. Bäuerle, K. Leo, *J. Appl. Phys.* **2008**, *104*, 074511.
[87] H. Minemawari, M. Tanaka, S. Tsuzuki, S. Inoue, T. Yamada, R. Kumai, Y. Shimoi, T. Hasegawa, *Chem. Mater.* **2017**, *29*, 1245.
[88] Y. Kikkawa, E. Koyama, S. Tsuzuki, K. Fujiwara, K. Miyake, H. Tokuhisa, M. Kanesato, *Surf. Sci.* **2007**, *601*, 2520.
[89] L. Ding, H.-B. Li, T. Lei, H.-Z. Ying, R.-B. Wang, Y. Zhou, Z.-M. Su, J. Pei, *Chem. Mater.* **2012**, *24*, 1944.
[90] X. Du, Y. Yuan, L. Zhou, H. Lin, C. Zheng, J. Luo, Z. Chen, S. Tao, L. Liao, *Adv. Funct. Mater.* **2020**, *30*, 1909837.
[91] R. Wang, J. Xu, L. Fu, C. Zhang, Q. Li, J. Yao, X. Li, C. Sun, Z.-G. Zhang, X. Wang, Y. Li, J. Ma, M. Xiao, *J. Am. Chem. Soc.* **2021**, *143*, 4359.
[92] F. C. Jamieson, E. B. Domingo, T. McCarthy-Ward, M. Heeney, N. Stingelin, J. R. Durrant, *Chem. Sci.* **2012**, *3*, 485.
[93] T. M. Clarke, C. Lungenschmied, J. Peet, N. Drolet, A. J. Mozer, *J. Phys. Chem. C* **2015**, *119*, 7016.
[94] Z. Jiang, *J. Appl. Crystallogr.* **2015**, *48*, 917.
[95] F. Kraffert, R. Steyrleuthner, C. Meier, R. Bittl, J. Behrends, *Appl. Phys. Lett.* **2015**, *107*, 043302.